

Title

Magnetic Resonance Image Processing Transformer for General Reconstruction

Authors/affiliations

Guoyao Shen ^{*[1, 2]}, Mengyu Li ^{*[1, 2]}, Stephan Anderson ^[2, 3], Chad W. Farris ^[3], Xin Zhang ^{† [1, 2]}

[1] Department of Mechanical Engineering, Boston University, Boston, MA 02215.

[2] The Photonics Center, Boston University, Boston, MA 02215.

[3] Department of Radiology, Boston Medical Center and Boston University Chobanian & Avedisian School of Medicine, Boston, MA, 02118.

* Equal contribution

†**Corresponding author:** Prof. Xin Zhang, email: xinz@bu.edu

Abstract

Purpose: To develop and evaluate a deep learning model for general accelerated MRI reconstruction.

Materials and Methods: This retrospective study built a magnetic resonance image processing transformer (MR-IPT) which includes multi-head-tails and a single shared window transformer main body. Three mutations of MR-IPT with different transformer structures were implemented to guide the design of our MR-IPT model. Pre-trained on the MRI set of RadImageNet including 672675 images with multiple anatomy categories, the model was further migrated and evaluated on fastMRI knee dataset with 25012 images for downstream reconstruction tasks. We performed comparison studies with three CNN-based conventional networks in zero- and few-shot learning scenarios. Transfer learning process was conducted on both MR-IPT and CNN networks to further validate the generalizability of MR-IPT. To study the model performance stability, we evaluated our model with various downstream dataset sizes ranging from 10 to 2500 images.

Result: The MR-IPT model provided superior performance in multiple downstream tasks compared to conventional CNN networks. MR-IPT achieved a PSNR/SSIM of 26.521/0.6102 (4-fold) and 24.861/0.4996 (8-fold) in 10-epoch learning, surpassing UNet128 at 25.056/0.5832 (4-fold) and 22.984/0.4637 (8-fold). With the same large-scale pre-training, MR-IPT provided a 5% performance boost compared to UNet128 in zero-shot learning in 8-fold and 3% in 4-fold.

Conclusion: MR-IPT framework benefits from its transformer-based structure and large-scale pre-training and can serve as a solid backbone in other downstream tasks with zero- and few-shot learning.

Main Body

Introduction

As a critical tool in non-invasive diagnosis, magnetic resonance imaging (MRI) provides precious diagnostic information. However, long acquisition times can hamper the availability and tolerability of these examinations for patients and lead to delays in diagnosis and nondiagnostic imaging, respectively. Compressed sensing is a common method to mitigate the long acquisition time of MRI by acquiring less measurement in k-space. Yet this downsampling often leads to misalignments and diminished image details. Numerous deep learning-based methods for accelerated MRI reconstruction [1-11] have been developed with superior performance. However, most are focusing on the model architecture design with a fixed acceleration factor and have limited generalizability. Few studies have the generalized ability to handle new types of images and different acceleration factors.

Deep learning-based models pre-trained on large-scale datasets have shown remarkable performance in multiple fields. Their effectiveness in multiple natural language processing tasks, computer vision, and cross-modality applications have shown great potential for general models [12-16]. Starting with the work of transformer [17], its architecture and variants have been widely adopted in various fields in natural language processing such as labelling, question-answering, translation, and more [12-16, 18,19]. Pre-trained transformer-based models on a large corpus have shown great generalizability. Later, vision transformer (ViT) brought this idea to image-related works by treating input images as patches, where each patch can be treated as a word similar to the transformer model [20-24]. Although the ViT model was designed for image recognition tasks in the beginning, masked autoencoder [25] further shows that the ViT-

based encoder and decoder can be used for image reconstruction tasks during pre-training to improve latent representation and benefits other downstream tasks such as classification and object detection, among others. Moreover, works such as the segment anything model [26] illustrates that ViT-based structure can be used as the backbone for more complex cross-modality models.

The aforementioned works demonstrate the generalizability of ViT-based models. More interestingly, image processing transformer (IPT) [27] proposes a multi-purpose model architecture by incorporating multiple heads and tails into the pre-training process with a single shared body. These different heads and tails serve as task-specific pre-encoders, allowing the main ViT body to focus on processing the flattened features and learning the connection among multiple low-level image tasks for better generalizability.

Although there have been numerous MRI reconstruction models, building a generalized MRI reconstruction model has been a challenging topic as the image deviates a lot as the acceleration factor changes. The information loss/degradation due to the k-space under-sampling is rather different from background noise such as Gaussian white noise, making techniques such as noise-to-noise (N2N) [28] learning infeasible. In this work, we present a magnetic resonance image processing transformer (MR-IPT) for general accelerated MRI reconstruction. We treat different under-sampling reconstructions as different tasks, enabling the main model body to concentrate on processing the flattened features and abstracting connections among different acceleration factors. We perform pre-training on a large-scale medical imaging dataset to excavate the model capability. Later, we perform tests on new

reconstruction tasks with different acceleration factors and datasets. Furthermore, we provide zero-shot and few-shot learning and comparisons with conventional reconstruction models to demonstrate the generalizability of the model. Our results show that MR-IPT exhibits superior performance even in zero-shot learning scenarios with a new dataset and can be fine-tuned to further fulfill higher performance needs. We hope that this work serves as a solid foundation for more generalized medical imaging methods in the future.

Materials and Methods

Datasets

This retrospective study used de-identified images that are publicly available. This study was therefore considered non-human subjects research with formal review waived by our institutional review board. We used two large-scale datasets: RadImageNet [29] and fastMRI [30]. The MRI subset of RadImageNet with 672675 total images was utilized and split into a training set with 605408 images for large-scale pre-training and a validation set with 67267 images for model design and tuning. After pre-training, we migrated to specific reconstruction tasks performed on the fastMRI knee dataset with 25012 MRI scans for downstream task transfer. The downstream tasks include finetune training on MRI reconstruction with two k-space perturbations: 4-fold acceleration via 0.08 center ratio, and 8-fold acceleration via 0.04 center ratio.

MR Image Processing Transformer

Figure 1 demonstrates the pipeline of our model. The overall structure consists of four components: heads, encoder, decoder, and tails. To process different imaging tasks, MR-IPT employs a multi-head structure, where each head handles a specific task separately. Consider an input image $x \in \mathbb{R}^{3 \times H \times W}$ (3 for an RGB image), each head generates a feature map.

$$f_H = H_i(x), i = \{1, 2, \dots, N_t\} \quad (1)$$

Where i denotes the i th task. $f_H \in \mathbb{R}^{C \times H \times W}$, C denotes the channel number for feature maps.

Similar to the vision transformer (ViT) model, f_H are reshaped into $N = \frac{HW}{P^2}$ patches $f_{p_i} \in \mathbb{R}^{C \times P^2}$, where P is the patch size. A position embedding is added to f_{p_i} and fed into the

transformer encoder-decoder structure. Similar to the heads as task-specific image encoder, tails work as task-specific decoder to output the final image.

$$f_T = T_i(f_D) \quad (2)$$

Where T_i denotes the i th task tail, $f_D \in \mathbb{R}^{C \times H \times W}$ is the decoded N patches from the decoder.

Consider an accelerated MR image x_{f_i} under the acceleration factor $f_i, i = \{1, 2, \dots, N_{acceleration}\}$ denotes the i th acceleration task. Then the head and tail for this acceleration reconstruction task can be denoted as:

$$f_H = H_{f_i}(x_{f_i}) \quad (3)$$

$$f_T = T_{f_i}(f_D) \quad (4)$$

The primary task of the model is to reconstruct MR images from 5 different levels of down-sampling strategies on k-space [34]: 2-fold acceleration with 0.1 center ratio, 4-fold acceleration with 0.08 center ratio, 6-fold acceleration with 0.06 center ratio, 8-fold acceleration with 0.04 center ratio and 10-fold acceleration with 0.02 center ratio. While acceleration increases and the center ratio decreases, the image becomes more corrupted and heavily misaligned. To pre-interpret the images and map them onto the desired dimension, five down-sampling accelerations are processed by five corresponding CNN blocks work as heads before entering a single shared encoder-decoder structure. Each head contains one CNN layer to map MRI scans of the dimension of $224 \times 224 \times 1$ into dimension of $224 \times 224 \times 64$, then followed by two CNN residual blocks to feed the intermediate vectors into the shared encoder-decoder structure. After being processed by encoder-decoder, intermediate vectors are then passed into

individual CNN blocks as tails with respect to their down-sampling accelerations. The objective of each tail aims to reconstruct clear images using original, unperturbed MRI scans as targets.

To efficiently train a large-scale transformer structure with reasonable efficiency, instead of directly deploying ViT [20], we utilize a window transformer structure [31] with several global attention blocks inserted in the encoder similar to a previously described approach [26]. Specifically, we sequentially deploy 24 transformer blocks with a window size of 14×14 , incorporating a local attention mechanism. For blocks 6, 12, 18, and 24, we use global attention instead and discard local attention in 14×14 windows. The transformer passes intermediate vectors with the embedding dimension of 1024 and 16 attention heads. On the other hand, the decoder is relatively lightweight compared to the encoder. It only contains 2 windowed transformer blocks followed by 2 transposed CNN blocks to upscale the intermediate embeddings back to $224 \times 224 \times 64$ dimension. In addition to the encoder-decoder structure, a separate prompt encoder was also attached to the model to map distinct labels indicating each head/tail into fixed embeddings. These label embeddings are also passed into the decoder by concatenating them with image embeddings. We train our model with an Adam optimizer [32] with a learning rate of $1e-5$ and L1 loss between prediction and target. During the pre-training, each input image is randomly assigned to a down-sampling strategy and perturbed in its k-space with the corresponding center ratio and acceleration. After the image is perturbed, it is fed into the overall model along with a label (ranging from 1 - 5) indicating which head/tail should be utilized. Due to the model's scale and hardware constraints, the batch size was set to 1, and the model was pre-trained for 5 epochs.

Statistical Analysis

Models were evaluated based on peak signal-to-noise ratio (PSNR) and structural similarity (SSIM) on their respective test sets. More specifically, PSNR and SSIM are calculated by comparing the fully sampled clean images and the reconstructed images from model outputs. Three MR-IPT mutations were evaluated with the overall best performance one as the final framework design. MR-IPT was pre-trained first on the RadImageNet dataset and then migrated to downstream reconstruction tasks for further fine-tuning on the training set. Three convolutional neural networks (CNNs) are implemented for comparison and trained on the training set. The most effective CNN served as a baseline in the second phase, where it adopted the same pre-training and fine-tuning procedures as the MR-IPT model, following comparison with the MR-IPT model for zero-shot and one-shot downstream task evaluations. To investigate the model performance regarding downstream dataset scale, we randomly sampled a subset from the training set, repeated this process ten times, and recorded their corresponding metrics and standard deviations. This dataset scale test was performed with six different sizes to mimic various usage scenarios.

Data and Code Availability

The RadImageNet dataset that support the findings of this study are openly available at: <https://www.radimagenet.com/>. The fastMRI dataset that support the findings of this study are openly available at: <https://fastmri.med.nyu.edu/>.

Results

Dataset Demographics

Two datasets were utilized in this study: RadImageNet [36] and fastMRI [34] datasets. For RadImageNet dataset, we used the MRI subset for pre-training. It includes 672675 de-identified images. We chose the knee dataset in fastMRI as our downstream dataset. It includes 25012 de-identified images. Patient demographics for both datasets were not released for public access.

MR-IPT Structure Comparisons

The multi-head-tail with a shared main body design offers much flexibility for detailed transformer design. We implemented three mutations for the MR-IPT framework: vanilla transformer, UNet transformer, and windowed transformer. All three mutations were trained on the validation set with performance shown in Figure 2. After a 5-epoch validation training, we chose the windowed transformer as our formal framework design with an SSIM of 0.6127, surpassing the UNet transformer at 0.6016 and the vanilla transformer at 0.5950.

MR-IPT Performance in Downstream Tasks

The downstream tasks include finetune training on MRI reconstructions with two k-space perturbations: 4-fold acceleration via 0.08 center ratio, and 8-fold acceleration via 0.04 center ratio [30]. For each task, the model was finetuned on the overall fastMRI knee dataset with (1) zero shot, (2) one epoch, and (3) ten epochs training iterations. In comparison, we use three UNet structures with 4 steps of contraction/expansion path [33]. Separately, they have number of input channels for the first layer being 32, 64, and 128. All three UNets are directly trained on

the fastMRI knee dataset with the same downstream tasks and the same training recipe as our MR-IPT model. The results shown in Table 1 indicate that a pre-trained MR-IPT model achieved an PSNR/SSIM of 24.722/0.5747 (4-fold) and 22.738/0.4481 (8-fold), which were even better compared to a trained UNet128 for 1 epoch at 24.218/0.5629 (4-fold) and 21.903/0.4379 (8-fold) and a UNet64 for 10 epochs at 24.233/0.5570 (4-fold) and 22.233/0.4565 (8-fold). When performed 10 epoch few-shot learning, MR-IPT achieved an PSNR/SSIM of 26.521/0.6102 (4-fold) and 24.861/0.4996 (8-fold) and outperformed the overall best CNN-based UNet128 at 25.056/0.5832 (4-fold) and 22.984/0.4637 (8-fold).

To further the generalizability of MR-IPT. We performed a parallel comparison with the UNet128, which has the best performance on tests in Table 1. In this part, UNet128 was pre-trained on the same RadImageNet dataset as MR-IPT and transferred to the same downstream tasks using fastMRI dataset for fine-tuning. The pre-training was done by randomly applying different sampling strategies to the input MRI images and then fed into the same UNet structure. Then the UNet128 was transferred to the same two downstream tasks as before. The test results are shown in Table 2. Our MR-IPT model outperforms UNet128 on all levels of reconstruction tasks. Interestingly, although a CNN-based UNet128 can still benefit from pre-training, the performance disparity increases in comparison to MR-IPT as the perturbation level increases. For example, in zero-shot learning, UNet128 achieved an PSNR/SSIM of 24.085/0.5603 (4-fold) and 21.662/0.4271 (8-fold) compared to MR-IPT at 24.722/0.5747 (4-fold) and 22.738/0.4481 (8-fold). MR-IPT provided a performance enhancement from around 2.5% in 4-fold scenario to 5% in 8-fold scenario. This difference may result from the lack of generalization ability of CNN structures, as they struggle to discern the task differences with

more intense degradation. Therefore, it fails to self-adjust to robustly handle multiple levels of reconstruction tasks simultaneously.

Robustness Evaluation with Different Dataset Scales

In most scenarios, it is difficult to obtain large-scale downstream datasets for a throughout training on CNN-based models. In conditions where only a handful of (normally hundreds) images are available, fine-tuning the MR-IPT onto a smaller dataset is assumed to be more practical. Previous tests have shown that the MR-IPT pre-trained on RadImageNet can outperform a well-trained Unet128 model on fastMRI dataset with zero- and few-shot fine-tuning on the entire fastMRI dataset. To further explore the performance of MR-IPT on various sizes of downstream datasets, we further fine-tuned our MR-IPT model on fastMRI subsets ranging from 10 to 2500 slices. The test was conducted by randomly sampling a fixed number of slices in the overall fastMRI knee dataset and training & evaluating a pre-trained MR-IPT model on them. The downstream task remained fixed: reconstructing images with 4-fold acceleration and 0.08 center ratio k-space down-sampling. We repeated the process 10 times for each chosen dataset size and calculated the max, min, mean, and error for each set of 10 recordings. From the result shown in Table 3, The SSIM and PNSR reach 0.6 and 26.2 after 500 slices while having the minimum standard derivation. Comparing this with the 1 epoch finetune training on Table 1 which has PSNR/SSIM at 26.405/0.6058, the model starts to achieve a similar performance level as fine-tuning on the overall dataset after utilizing only 500 slices. Figure 3 plots the mean and standard deviation with different slice numbers to show the tendency. The result shows that: (1) the performance starts to converge after 100 slices of training dataset; (2) The MR-IPT structure outperforms a directly trained UNet128 (Table 1) after 100 slices.

Moreover, when the dataset size drops to 50 or 10, the performance of MR-IPT becomes highly dependent on the quality of the fine-tuning datasets. The bars depicted in Figure 2 indicate that the evaluation uncertainty on SSIM and PSNR indexes increases while the dataset size decreases from 100 to 10 slices.

Discussion

Despite recent advancements in deep learning-based models for medical imaging reconstructions, these studies also highlight significant limitations: conventional deep neural networks require training on specific datasets and can lack generalizability when migrated to another dataset. Differences in imaging conditions, hardware, and anatomy being imaged can lead to unstable performance, especially for CNN-based networks due to their limitations in latent representations. To address this, we proposed a magnetic resonance image processing transformer (MR-IPT) for general accelerated MRI reconstruction. Different from conventional deep-learning-based medical imaging models for MRI reconstruction, MR-IPT includes a multi-heads-tails structure with a shared main skeleton to handle different acceleration setups.

Thanks to the latent presentation potential inherited in the transformer structure, the shared main skeleton is capable of learning the correlation among multiple reconstruction tasks. The shared encoder-decoder main body also provides much flexibility for model design. We implemented three transformer mutations: vanilla, UNet-based, and windowed transformer. By evaluating their performance through training on the same fastMRI dataset, we chose the best-performing windowed transformer as our formal structure.

Transformer-based models typically require larger datasets for training to fully excavate their potential. In this work, we performed pre-training on RadImageNet with 60548 MR images with multiple anatomy categories including knee, shoulder, spine, ankle/foot, abdomen/pelvis, brain and hip. MR-IPT achieved superior performance in downstream tasks on another fastMRI knee dataset including 67267 images, even with zero-shot learning. Our model reached an PSNR/SSIM

of 24.722/0.5747 (4-fold) and 22.738/0.4481, which outperformed a specifically trained UNet64 at 10 epochs with a PSNR/SSIM of 24.233/0.5570 (4-fold) and 22.233/0.4565 (8-fold).

With few-shot learning, MR-IPT provided superior performance in downstream tasks and outperformed CNN-based networks such as a UNet128. In our one-shot tests, MR-IPT achieved a PSNR/SSIM of 26.405/0.6508 (4-fold) and 24.681/0.4934 (8-fold), compared to an overall best CNN-based UNet128 at 24.218/0.5629 (4-fold) and 21.903/0.4379 (8-fold). In 10-epoch training tests, MR-IPT achieved a PSNR/SSIM of 26.521/0.6102 (4-fold) and 24.861/0.4996 (8-fold), compared to the UNet128 at 25.056/0.5832 (4-fold) and 22.984/0.4637 (8-fold). Benefiting from the shared transformer-based main body, MR-IPT can further excavate the potential of large-scale datasets. We chose UNet128 as a CNN-based baseline model, performed the same large-scale pretraining, and conducted zero- and single-shot down-stream evaluation compared to MR-IPT. Our results show that MR-IPT provides an enhancement of 3-5% in both cases. Notably, the enhancement is more obvious as the perturbation level increases (Table 2). This indicates that CNN-based models are more dependent on the downstream training especially when acceleration factors are higher.

To evaluate MR-IPT's capability in clinical cases where datasets are rather limited, model performance stability was studied as well in this work. We randomly picked a subset from the whole downstream dataset and repeatedly recorded the model performance with their standard deviations. MR-IPT achieved a similar level of performance compared to that achieved through fine-tuning on the entire downstream dataset, using only 500 images. We also noted

that as the dataset scale went smaller, the performance became more unstable and more dependent on the dataset (Table 3, Figure 3).

We do notice limitations of our study. MR-IPT was exclusively pre-trained with the MRI subset without other imaging types such as CT and ultrasound. Consequently, the MR-IPT is expected to be widely generalizable to a wide range of MR imaging, but its generalizability to other imaging modalities, such as CT or US may be limited. In addition, our work is limited to accelerated MRI reconstructions. Other low-level imaging tasks such as denoising, segmentation, and super-resolution would require an even broader range of pre-training. Moreover, the dataset cohorts we use come from only two public sources with RadImageNet for pretraining and fastMRI for validation. Although they might be sufficient to prove the feasibility of our model, future tests can also be expanded by pretraining/transferring MR-IPT on other public medical image datasets. Additionally, MR-IPT's framework still requires separate heads and tails, which could limit the expandability as the downstream task types increase. Though we have a specific prompt encoder for acceleration settings in our design, further work could focus on co-training image encoders and prompt encoders with techniques such as masked-autoencoders [25] and CLIP [34] so that the encoders become more universal.

In conclusion, we proposed a Magnetic Resonance Image Processing Transformer (MR-IPT) for general accelerated MRI reconstruction. It benefits from the transformer-based structure and large-scale pre-training. We demonstrated that MR-IPT outperformed conventional CNN-based networks in multiple downstream tasks with zero- and few-shot learning. Our results also showed that MR-IPT can provide stable performance with rather limited downstream dataset

scales. With proper pre-training, MR-IPT could serve as a solid framework or backbone in addressing other downstream tasks.

References

1. Eo T, Jun Y, Kim T, Jang J, Lee H-J, Hwang D. KIKI-net: cross-domain convolutional neural networks for reconstructing undersampled magnetic resonance images. *Magnetic Resonance in Medicine* 2018 80:2188–2201. doi: 10.1002/mrm.27201
2. Sriram A, Zbontar J, Murrell T, Zitnick CL, Defazio A, Sodickson DK. GrappaNet: combining parallel imaging with deep learning for multi-coil MRI reconstruction. In: *Proceedings of the IEEE/CVF Conference on Computer Vision and Pattern Recognition (CVPR) 2020*. doi: 10.1109/CVPR42600.2020.01432
3. Lin K, Heckel R. Vision Transformers Enable Fast and Robust Accelerated MRI. In: *Proceedings of the 5th International Conference on Medical Imaging with Deep Learning 2022*. PMLR, pp 774–795.
4. Shen G, Li M, Farris CW, Anderson S, Zhang X. K-space Cold Diffusion: Learning to Reconstruct Accelerated MRI without Noise. arXiv 2311.10162 [preprint] <https://arxiv.org/abs/2311.10162>. Published February 16, 2024. Accessed April 25, 2024.
5. Souza R, Frayne R. A Hybrid Frequency-Domain/Image-Domain Deep Network for Magnetic Resonance Image Reconstruction. In: *2019 32nd SIBGRAPI Conference on Graphics, Patterns and Images (SIBGRAPI) 2019*. pp 257–264. doi: 10.1109/SIBGRAPI.2019.00042
6. Souza R, Bento M, Nogovitsyn N, Chung KJ, Loos W, Lebel RM, Frayne R. Dual-domain cascade of U-nets for multi-channel magnetic resonance image reconstruction. *Magnetic Resonance Imaging* 2020 71:140–153. doi: 10.1016/j.mri.2020.06.002

7. Schlemper J, Caballero J, Hajnal JV, Price AN, Rueckert D. A Deep Cascade of Convolutional Neural Networks for Dynamic MR Image Reconstruction. *IEEE Transactions on Medical Imaging* 2018 37:491–503. doi: 10.1109/TMI.2017.2760978
8. Hammernik K, Klatzer T, Kobler E, Recht MP, Sodickson DK, Pock T, Knoll F. Learning a variational network for reconstruction of accelerated MRI data. *Magnetic Resonance in Medicine* 2018 79:3055–3071. doi: 10.1002/mrm.26977
9. Sriram A, Zbontar J, Murrell T, Defazio A, Zitnick CL, Yakubova N, Knoll F, Johnson P. End-to-End Variational Networks for Accelerated MRI Reconstruction. In: *Medical Image Computing and Computer Assisted Intervention – MICCAI 2020*. Springer, pp 64–73
10. Shen G, Hao B, Li M, Farris CW, Paschalidis ICh, Anderson SW, Zhang X. Attention hybrid variational net for accelerated MRI reconstruction. *APL Machine Learning* 2023 1:046116. doi: 10.1063/5.0165485
11. Montalt-Tordera J, Muthurangu V, Hauptmann A, Steeden JA. Machine learning in Magnetic Resonance Imaging: Image reconstruction. *Physica Medica* 2021 83:79–87. doi: 10.1016/j.ejmp.2021.02.020
12. Devlin J, Chang M-W, Lee K, Toutanova K. BERT: Pre-training of Deep Bidirectional Transformers for Language Understanding. arXiv 1810.04805 [preprint] <https://arxiv.org/abs/1810.04805>. Published May 24, 2019. Accessed April 25, 2024.
13. Brown T, et al. Language Models are Few-Shot Learners. In: *Advances in Neural Information Processing Systems 2020*, vol. 33, pp 1877–1901
14. Radford A, Narasimhan K, Salimans T, Sutskever I. Improving language understanding by generative pre-training. OpenAI research 2018.

15. Ouyang L, et al. Training language models to follow instructions with human feedback. In: Advances in Neural Information Processing Systems 2020, vol. 35, pp 27730–27744
16. Radford A, Wu J, Child R, Luan D, Amodei D, Sutskever I. Language models are unsupervised multitask learners. OpenAI blog 2019.
17. Vaswani A, et al. Attention is all you need. In: Advances in Neural Information Processing Systems 2017, vol. 30.
18. Lin T, Wang Y, Liu X, Qiu X. A survey of transformers. AI Open 2022, vol. 3, pp. 111–132. doi: 10.1016/j.aiopen.2022.10.001
19. Tay Y, Dehghani M, Bahri D, Metzler D. Efficient transformers: a survey. ACM Comput. Surv. 2022, vol. 55, no. 6. doi: 10.1145/3530811
20. Dosovitskiy A, et al. An image is worth 16x16 words: transformers for image recognition at scale. arXiv 2010.11929 [preprint] <https://arxiv.org/abs/2010.11929>. Published June 3, 2021. Accessed April 25, 2024.
21. Bao H, Dong L, Piao S, Wei F. BEiT: BERT pre-training of image transformers. arXiv 2106.08254 [preprint] <https://arxiv.org/abs/2106.08254>. Published September 3, 2022. Accessed April 25, 2024.
22. Zhou D, et al. DeepViT: towards deeper vision transformer. arXiv 2103.11886 [preprint] <https://arxiv.org/abs/2103.11886>. Published April 19, 2021. Accessed April 25, 2024.
23. Li Y, Mao H, Girshick R, He K. Exploring plain vision transformer backbones for object detection. In: Computer Vision - ECCV 2022, pp. 280–296. doi: 10.1007/978-3-031-20077-9_17

24. Han K, et al. A survey on vision transformer. In: IEEE Transactions on Pattern Analysis and Machine Intelligence 2023, vol. 45, no. 1, pp. 87-110. doi: 10.1109/TPAMI.2022.3152247
25. He K, Chen X, Xie S, Li Y, Dollár P, Girshick R. Masked autoencoders are scalable vision learners. In: Proceedings of the IEEE/CVF Conference on Computer Vision and Pattern Recognition (CVPR) 2022, pp. 16000–16009.
26. Kirillov A, et al. Segment anything. In: Proceedings of the IEEE/CVF International Conference on Computer Vision (ICCV) 2023, pp. 4015–4026.
27. Chen H, et al. Pre-trained image processing transformer. In: Proceedings of the IEEE/CVF Conference on Computer Vision and Pattern Recognition (CVPR) 2021, pp. 12299–12310.
28. Gan W, Sun Y, Eldeniz C, Liu J, An H, Kamilov US. Deformation-compensated learning for image reconstruction without ground truth. In: IEEE Transactions on Medical Imaging 2022, vol. 41, no. 9, pp. 2371-2384. doi: 10.1109/TMI.2022.3163018
29. Mei X et al. RadImageNet: an open radiologic deep learning research dataset for effective transfer learning. Radiology: Artificial Intelligence 2022, vol. 4, no. 5, p. e210315. doi: 10.1148/ryai.210315
30. Zbontar J, et al. fastMRI: An open dataset and benchmarks for accelerated MRI. arXiv 1811.08839 [preprint] <https://arxiv.org/abs/1811.08839>. Published December 11, 2019. Accessed April 25, 2024.
31. Liu Z, et al. Swin transformer: hierarchical vision transformer using shifted windows. In: Proceedings of the IEEE/CVF International Conference on Computer Vision (ICCV) 2021, pp. 10012–10022.

32. Kingma DP, Ba J. Adam: A method for stochastic optimization. arXiv 1412.6980 [preprint]
<https://arxiv.org/abs/1412.6980>. Published January 30, 2017. Accessed April 25, 2024.

33. Ronneberger O, Fischer P, Brox T. U-net: Convolutional networks for biomedical image segmentation. In: Medical Image Computing and Computer-Assisted Intervention–MICCAI 2015: 18th International Conference, Munich, Germany, October 5-9, 2015, Proceedings, Part III 18, pages 234–241. doi: 10.1007/978-3-319-24574-4_28

34. Radford A, et al. Learning transferable visual models from natural language supervision. In: Proceedings of the 38th International Conference on Machine Learning 2021, vol. 139, pp. 8748–8763

Figures and Legends

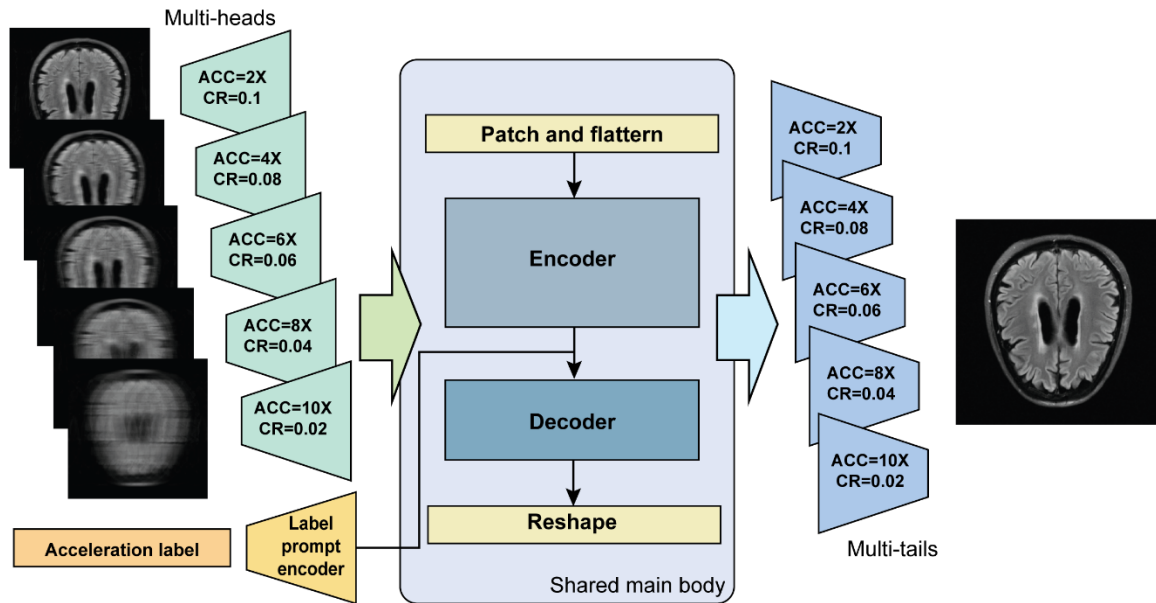


Figure 1. The overall structure of our MR-IPT framework. It includes a multi-head-tails design for different under-sampling setups. The shared main body consists of an encoder and a light decoder. A separate prompt encoder was also attached to the model to map distinct labels indicating each heads/tail into fixed embeddings.

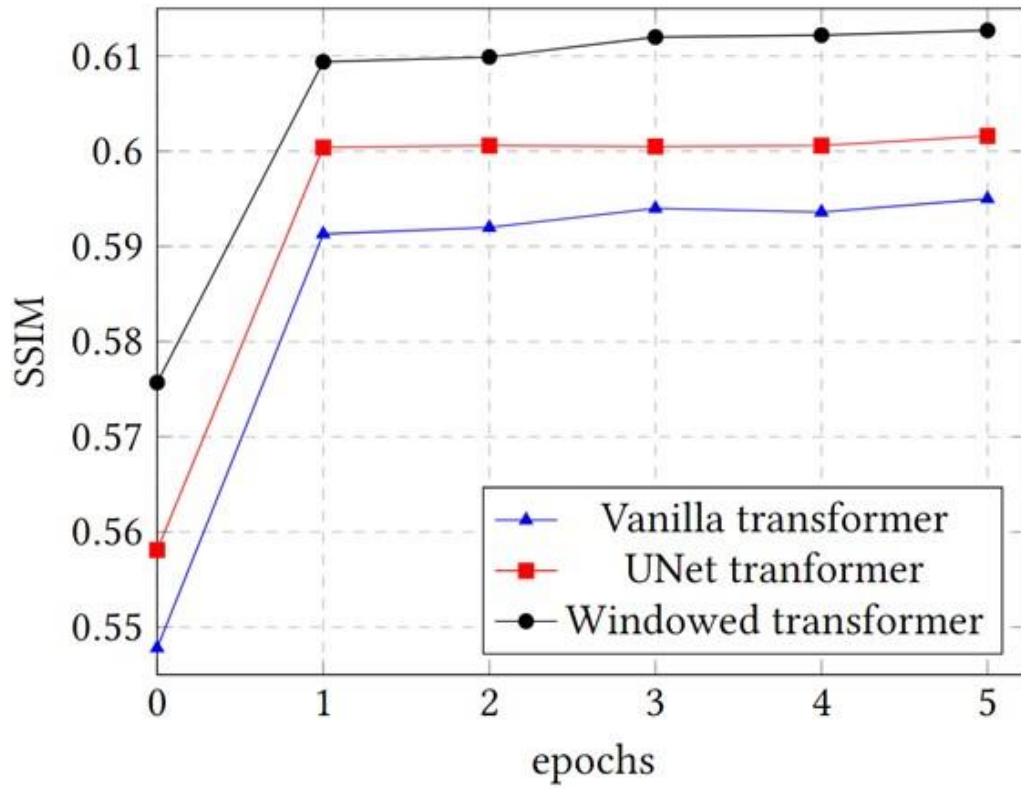


Figure 2. MR-IPT mutations performance comparison. Three versions of MR-IPT were implemented and validated. We chose windowed transformer as our final structure design.

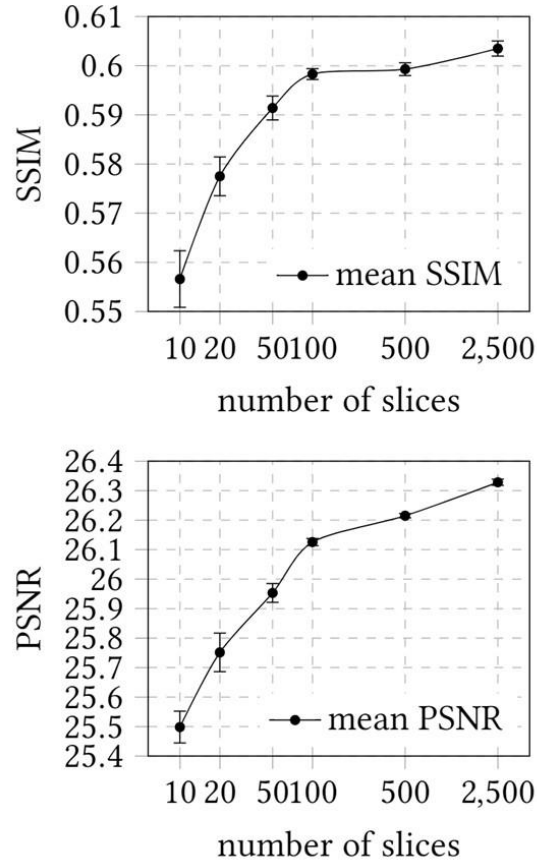


Figure 3. MR-IPT performance with different down-stream task dataset sizes. We repeated the process 10 times for each chosen dataset size and calculate the max, min, mean and standard deviation for each set of 10 recordings. The error bar indicates the standard deviation for each dataset size correspondingly.

Tables

Epoch	Evaluation	ACC=4X, CR=0.08				ACC=8X, CR=0.04			
		UNet32	UNet64	UNet128	MR-IPT	UNet32	UNet64	UNet128	MR-IPT
0	PSNR				24.722				22.738
	SSIM				0.5747				0.4481
1	PSNR	22.664	22.914	24.218	26.405	21.548	22.913	21.903	24.681
	SSIM	0.5166	0.5245	0.5629	0.6058	0.4130	0.4308	0.4379	0.4934
10	PSNR	23.871	24.233	25.056	26.521	22.518	22.233	22.984	24.861
	SSIM	0.5502	0.5570	0.5832	0.6102	0.4479	0.4565	0.4637	0.4996

Table 1. Quantitative metrics for comparison between multiple scales of UNet structure and MR-IPT model pretrained on RadImageNet dataset. Two finetune tasks including reconstruction of 4-fold acceleration with 0.08 center ratio (CR) and 8-fold acceleration with 0.04 center ratio degraded MRIs. Numbers in bold face indicate the best metrics out of all the models.

Epoch	Degradation	Evaluation	UNet128	MR-IPT	Enhancement
0	4X, 0.08	PSNR	24.085	24.722	2.64%
		SSIM	0.5603	0.5747	2.57%
	8X, 0.04	PSNR	21.662	22.738	4.97%
		SSIM	0.4271	0.4481	4.91%
1	4X, 0.08	PSNR	25.657	26.405	2.92%
		SSIM	0.5868	0.6058	3.24%
	8X, 0.04	PSNR	23.234	24.681	6.22%
		SSIM	0.4763	0.4934	3.59%

Table 2. Quantitative metrics for comparison between MR-IPT and CNN model, both pretrained on RadImageNet dataset, by their performance on reconstruction tasks using fastMRI knee dataset.

# slices	Evaluation	Max	Min	Mean	STD $\times 10^{-3}$
10	PSNR	25.5998	25.3634	25.4983	53.92
	SSIM	0.5731	0.5566	0.5588	5.755
20	PSNR	25.8275	25.7265	25.7515	65.42
	SSIM	0.5863	0.5772	0.5775	3.948
50	PSNR	25.9804	25.9381	25.9532	31.81
	SSIM	0.5933	0.5890	0.5914	2.431
100	PSNR	26.1360	26.0260	26.1256	12.07
	SSIM	0.5985	0.5931	0.5983	1.107
500	PSNR	26.2637	26.1000	26.2150	7.24
	SSIM	0.6018	0.5990	0.5993	1.299
2500	PSNR	26.3452	26.3112	26.3284	10.05
	SSIM	0.6053	0.5998	0.6035	1.855

Table 3. Pretrained MR-IPT performance on different dataset size on fastMRI. The dataset size increasing from 10 to 2500 slices. For each dataset size, the downstream training was repeated 10 times and mean, max, min, std for PNSR and SSIM are recorded.

Acknowledgements

This work is supported by the Rajen Kilachand Fund for Integrated Life Science and Engineering. We would like to thank the Boston University Photonics Center for technical support.

Author declarations section

1. Conflict of interests

The authors have no conflicts of interest to disclose.

2. Ethics approval statement

No animal or human experiments are included in this work.

3. Author contributions

Guoyao Shen: Conceptualization (equal); Methodology (equal); Software (equal); Formal Analysis (equal); Writing – Original Draft (lead). **Mengyu Li:** Methodology (equal); Software (equal); Formal Analysis (equal); Writing – Original Draft (supporting). **Stephan Anderson:** Methodology (supporting); Writing – Review & Editing (equal). **Chad W. Farris:** Conceptualization (supporting); Formal Analysis (supporting); Writing – Review & Editing (supporting). **Xin Zhang:** Conceptualization (equal); Methodology (supporting); Software (supporting); Formal Analysis (supporting); Writing – Review & Editing (equal); Project Administration (lead); Funding Acquisition (lead).